

# Journal of the Geological Society

## Centennial to decadal vegetation community changes linked to orbital and solar forcing during the Dan-C2 hyperthermal event.

--Manuscript Draft--

<b>Manuscript Number:</b>	jgs2017-022R1
<b>Article Type:</b>	Research article
<b>Full Title:</b>	Centennial to decadal vegetation community changes linked to orbital and solar forcing during the Dan-C2 hyperthermal event.
<b>Short Title:</b>	Vegetation change,Dan-C2 hyperthermal
<b>Corresponding Author:</b>	David William Jolley, B.Sc.(Hons), M.Sc. Ph.D. University of Aberdeen Aberdeen, Aberdeen UNITED KINGDOM
<b>Corresponding Author E-Mail:</b>	d.jolley@abdn.ac.uk
<b>Other Authors:</b>	Robert James Daly Alena Ebinghaus David Kemp Iain Gilmour Conall MacNiocaill Simon Kelley
<b>Manuscript Classifications:</b>	Palaeoclimatology; Palaeoenvironments; Palaeontology and geobiology
<b>Additional Information:</b>	
<b>Question</b>	<b>Response</b>
Are there any conflicting interests, financial or otherwise?	No
Samples used for data or illustrations in this article have been collected in a responsible manner	Confirmed
<b>Response to Reviewers:</b>	

# **Centennial to decadal vegetation community changes linked to orbital and solar forcing during the Dan-C2 hyperthermal event.**

D.W.Jolley<sup>1\*</sup>, R.J.Daly<sup>1</sup>, A. Ebinghaus<sup>1</sup>, D. B. Kemp<sup>1</sup>, I. Gilmour<sup>2</sup>, C. Mac Niocaill<sup>3</sup> and S.P. Kelley<sup>2</sup>

1. Department of Geology & Petroleum Geology, School of Geosciences, University of Aberdeen, King's College, Aberdeen AB24 3UE, UK

2. Open University, Faculty of Science Technology & Engineering, Walton Hall, Milton Keynes.

3. Department of Earth Sciences, South Parks Road, Oxford OX1 3AN, UK

\* corresponding author

## **Abstract**

Formed close to the K/Pg boundary, the Boltsh meteorite crater, Ukraine, preserves >400m of lacustrine sedimentary rocks which include a record of the early Danian Dan-C2 hyperthermal event. Abundant pollen, spores and algae recovered from these sediments have yielded a cyclic record of plant ecology change paced by ~21ky orbital precession cycles. New, higher resolution sampling across the inception of the Dan-C2 hyperthermal event has identified oscillations in vegetation community ecology at sub-orbital periods of ~2 ky, ~200 y, and ~11 y. These are consistent with possible Hallstatt, DeVreiss/Suess, and Schwabe solar cycles, respectively. Rapid regime shift from savanna to a mesic forest ecosystems was paced by ~21ky precession, with the shift likely occurring in <200y. Prior to regime shift, ~2 ky (i.e. possible Hallstatt) oscillations between mesic- and winterwet-dominated plant communities increased in intensity, suggestive of ecological flickering.

*Supplementary material (detrended correspondence, and changepoint analysis, palynological frequency data for DCA groups and core photographs) is available at*

## **Introduction**

Hyperthermal events represent some of the most extreme changes in Earth's surface conditions of the past 200 Ma, and are associated with transient increases in global temperatures (typically  $\sim 5^{\circ}\text{C}$ ), changes in  $p\text{CO}_2$ , changes in hydrology, mass extinction, and ocean acidification and deoxygenation (e.g. Zeebe & Zachos, 2013). Hyperthermals such as the PETM ( $\sim 56$  Ma), early Toarcian ( $\sim 182$  Ma) and early Aptian ( $\sim 120$  Ma) have been considered to be Earth system analogues for anthropogenic warming scenarios, because there is evidence that warming during these events was associated with the transfer of large amounts ( $>10^3$  petagrams) of carbon to the oceans and atmosphere (Kemp et al., 2005; Mehay et al., 2009; Kirtland Turner & Ridgwell, 2013; Alexander et al., 2015; Zeebe et al., 2014). Despite the utility of studying these events, uncertainties in age models and the limited resolution of the geological record has hindered the comparison of these deep time events with anthropogenic climate change. This uncertainty has been compounded by recent suggestions that warming occurred at rates orders of magnitude slower than anthropogenic forced change (Zeebe et al., 2016).

An essential part of elucidating the nature of hyperthermals and evaluating their impact on life on Earth is the acquisition and study of complete, high fidelity records. Notably, there is a general lack of non-marine records of ancient hyperthermals, and those that do exist are typically of relatively lower fidelity compared to marine records (e.g. Hesselbo & Pieńkowski 2011; Abels et al., 2012). The paucity of high fidelity terrestrial archives hinders our ability to define the response of continental ecosystems and hydrology to ancient warming.

The lacustrine sedimentary rock record preserved in the Boltysh Impact Crater, Ukraine (Jolley et al, 2010, 2013; Gilmour et al., 2013) preserves one such high fidelity record of the early Danian Dan-C2 hyperthermal event (~65 Ma). Here, evidence for the impact of the Dan-C2 hyperthermal event on plant ecosystems is examined, and uncoupled from evidence for orbital (Jolley et al., 2015) and solar forcing.

### **The Boltysh Impact Crater record of the Dan-C2 hyperthermal event**

In the 0.5 my following the Cretaceous/Palaeogene (K/Pg) boundary, ~400m of sediments were deposited in the Boltysh Impact Crater lake (48.9°N 32.25°E Figure 1) at rates of ~0.8 mm y<sup>-1</sup>, creating a globally unique and detailed record of the early Danian Earth system (Figure 2). Initial investigations of the cores recovered from drilling the crater sediments in 2008 (Hole 42/11) identified a unique record of both the K/Pg transition and the Dan-C2 hyperthermal event (Jolley et al., 2010; 2013, 2015; Gilmour et al., 2013; 2014). What makes the Boltysh Crater record of fundamental importance is that it records the Dan-C2 hyperthermal event at a resolution comparable to modern lake sediments Gilmour et al., 2013, 2014, (Figure 2). Moreover, it is the only non-marine record of this event yet studied. Through our previous analyses (Gilmour et al., 2013; 2014; Jolley et al., 2015), coupled with work by others on marine records of the Dan-C2 event (Quillévéré et al., 2008; Coccioni et al., 2010), it has been established that there are similarities between the Dan-C2 and the PETM and early Toarcian hyperthermals. Notably, all three events are characterised by transient negative C-isotope excursions (CIEs) likely associated with the emission of large amounts of <sup>12</sup>C, and pronounced warming (Gilmour et al., 2013; Kemp et al., 2005; Zeebe & Zachos, 2013; Hesselbo et al., 2000; Quillévéré, 2008). Additionally, all three CIEs appear to have been paced at least in part by orbital forcing, and coincided with episodes of large-

scale volcanism (Gilmour et al., 2013, 2014; Kemp et al., 2005; Lunt et al., 2011). Unlike marine records of the Dan-C2 event, the Boltysh CIE resembles the form of the most detailed records of the Toarcian and PETM (Jolley et al., 2015). However, in comparison to these better-known hyperthermals, the Boltysh Dan-C2 CIE occurs in often laminated, unbioturbated sediments that are close to an order of magnitude thicker than the most expanded Toarcian and PETM records (Figure 2).

A previously published C-isotope record (Gilmour et al., 2013) through the Dan-C2 in Boltysh revealed a negative excursion of ~3‰ in bulk organic matter spanning ~200 m of strata (Figure 2). Statistically significant (>99% confidence level) ~30 m cycles were recognized (Figure 2) in these raw C-isotope data (Gilmour et al., 2013). Based on correlation to marine records, these cycles were attributed to the influence of either precession (~21 ky) or obliquity (~40 ky) orbital forcing (Gilmour et al., 2013; see also Gilmour et al., 2014). Variations in palynoflora through the Boltysh record have been interpreted as a sequence of moisture availability cycles (MAO's; Jolley et al., 2013, 2015), which occur at a frequency comparable to the cyclicity observed in the carbon isotope record (Jolley et al., 2015 and Figure 2). These MAO's represent alternation between winterwet (warmer, dryer) and mesic forest (cooler, wetter) vegetation biomes.

Further temporal constraint on these cycles and the succession has recently become available from a pilot study of sedimentary rock palaeomagnetism, which has established the approximate position of the C29r/C29n magnetic reversal in the Boltysh core (Figure 2). These data corroborate the earlier correlation of Gilmour et al. (2013, 2014) of the Boltysh CIE with the marine Dan-C2 event, and demonstrate that the Boltysh strata span ~1 my of the early Danian from the K/Pg (66.00Ma;  $66.043 \pm 0.043$  in Sprain et al. 2015, see also Dinares-Turell et al., 2014) to within C29n (Figure 2). The base of C29n ( $65.832 \pm 0.036$ ,

Sprain et al., 2015) has been positioned by our palaeomagnetic analysis and by correlation to records from holes DSDP 528 and DSDP 527 (Quillévéré, 2008, Figure 2) and occurs within Stage 3 of the Boltysh CIE (Figure 2). Comparison to the record of MAO's in post K/Pg boundary Chron 29r sediments of the Boltysh crater fill (Jolley et al., 2015) identified eleven cycles from the K/Pg boundary to the base of C29n. Using isotopic dating of the K/Pg boundary and of the base of C29n (Sprain et al., 2015) the post K/Pg C29r interval is ~211 ky. This duration is in accordance with that proposed by Dinares-Turell et al. (2014 and Figure 2). Eleven MAO's have been recognized over the K/Pg boundary to base C29n interval in the Boltysh 42/11 palynology record (Figure 2). Accordingly, ascribing MAO's to 21 ky solar cycles yields a duration of ~231 ky (21 ky x 11 MAO cycles) for this interval, in close agreement with Sprain et al. (2015) (Figure 2). Similarly, the interval from the inception of the Dan-C2 CIE to the base of C29n spans approximately six ~30 m cycles in C-isotopes (Gilmour et al., 2013) providing a similar age calibration.

#### **Assessing the nature and rate of ecosystem change**

Stratigraphically abrupt composition changes were recorded in the Boltysh palynofloral data, particularly at boundaries between the MAO's (Jolley et al., 2015). Given the time constraints outlined above, these compositional shifts are interpreted as responses to ~21 ky orbital precession forcing, showing a correlation with the carbon isotope cyclicity presented by Gilmour et al., (2014). Notably, one of these compositional shifts occurs coincident with the inception of the Dan-C2 CIE. Importantly, this rapid shift in palynofloral composition at the MAO4/MAO5 boundary spans a fraction of a ~21 ky cycle, and hence records a rapid response to climatic change at a sub-orbital, and perhaps anthropogenic-scale, tempo.

To assess the potential for using the Boltysh Dan-C2 record to inform our understanding of vegetation and climate change at potentially human-relevant timescales, it was necessary to carry out palynofloral and geochemical investigations at a temporal resolution beyond that derived from the ~1 m spaced sample data of Jolley et al (2015). Thus, a new sample set was collected at 0.3 m intervals and analysed for palynofloras and organic C-isotopes. Deriving a multi-centennial record from these samples was targeted at elucidating plant ecosystem dynamics across the boundaries between MAO's and between the wet-cool to warm-dry intervals within the ~21 ky MAO cycles. To obtain a record with a decadal resolution comparable to anthropogenic change, four further intervals of finely laminated sediment were sampled at 0.05 m – 0.06 m spacing. Finally, a single interval of 96 consecutive sub-mm laminations were separated and subjected to palynological analysis (Figure 3). All samples were processed following the methodology outlined in Jolley et al (2015), with the addition of an exotic spore standard and aliquot slide mounts.

### **Vegetation dynamics at MAO Boundaries**

Palynological analysis of 0.3 m spaced samples from the later, dryer phase of MAO4, throughout MAO5 into the early wetter phase of MAO6 recovered a rich and diverse palynoflora (Figure 3), consistent with other terrestrial early Danian successions (Jolley et al., 2015; Daly & Jolley, 2015). Pollen and spores dominate the palynofloras, but chlorophycean algae are also present, particularly in the dryer phases of MAO4 and MAO5. Acquisition of these data has allowed comparison of the rate and magnitude of change at both the MAO4/MAO5 boundary (coincidental with the CIE inception, Gilmour et al., 2013), and at the MAO5/MAO6 boundary within the isotope excursion (Figure 3)

Following normalization and data reduction (removal of taxa comprising <10% of total flora), the palynofloral data were subjected to detrended correspondence analysis (DCA). Results of this analysis were used to define groups of taxa with similar spatial distributions (Figure 3 and online data). The ecological significance of these groupings was assessed with reference to their botanical affinity and to previous ecological analyses (Jolley et al., 2015). Similar to previous analyses of the entire section (Jolley et al 2015), moisture availability and land surface temperature are reflected in the first two axes of this analysis.

Stratigraphical plots of the DCA derived communities from analysis of the 0.3 m spaced data showed apparently rapid ecological turnover at the boundaries between MAO4 and MAO5. A major compositional shift from dominance by mesic communities (Mesic Forest and Mesic Swamp groupings) to dominance by winter wet communities (mid succession Normapolles, Normapolles 1 and Normapolles 2 groupings) occurs over 30cm (480.9m to 481.2m). A subsequent comparable period of rapid change was identified at the MAO 5 – MAO6 boundary (Jolley et al., 2015), where a similar shift in palynofloral composition (Figure 3) occurs over 0.3 m (454.19m – 454.49m). The relative significance of these changes was tested using changepoint analysis (Gallagher et al, 2011: Supplementary online data) on DCA axis 1.

DCA of the 0.3 m data set revealed short frequency (~2.5 m) oscillations reflecting changes in moisture availability and diversity (Figure 3). Each cycle comprises a cooler, wetter early phase characterized by mesic forest taxa and lower DCA axis 1 values, followed by a later dryer and warmer phase characterized by savanna assemblages. Spectral analysis ( $2\pi$  multitaper) indicates cyclicity in the DCA axis 2 data with a period of ~2.6 m (Figure 3). Considering the orbital chronology, the approximate duration of these cycles is ~2 ky (~12 cycles per 30 m precession (21 ky) cycle), and thus potentially consistent with solar



Hallstatt cycles (~2.1-2.5 ky period; within the bandwidth error of the observed DCA axis 2 cycle period) (e.g. Damon and Sonett, 1991; Kern et al., 2012; Lenz et al., 2016). Also evident from the frequency plots of ordination groups (Figure 3) are intervals of rapid and significant change in palynofloral composition. These are also indicated from changepoint analysis (Supplimentary data) which shows the ~21 ky precession cycles, as well as shorter periodicity changes spanning approximately four ~2.5 m cycles. These unknown ~8 ky periods do not display clear cyclicity in their palynofloras, the boundaries within 21ky cycles marking shifts to lower moisture availability floras. Both the 21ky and ~8 ky shifts in palynofloral composition are not necessarily evidence of abrupt changes in climate or forcing. Instead, they represent two different magnitudes of shift in parent flora ecology where cumulative forcing overcame plant community resilience to environmental change. The relative magnitude of these shifts is most readily apparent from the projection of the data on a time axis (Figure 4), highlighting the potential correlation of rapid palynofloral compositional shifts to hypothetical forcing.

### **An anthropogenic-scale record of vegetation change**

While data derived from the 0.3 m spaced samples across the inception of the Dan-C2 CIE has enabled identification of second (~8 ky) and third (~2 ky) order oscillations, these data are still of insufficient resolution to elucidate vegetation change at a rate comparable to anthropogenic climate forcing. Repeated intervals of the core, however, are composed of laminated organic-rich mudstone, and this has permitted high fidelity, closely-spaced sampling. Accordingly, four intervals were selected with sample spacing adjusted based on recognition of preliminary thicknesses of the ~2 ky units, varying between 0.05 m and 0.06m. Two intervals were chosen from the later stage of MAO4 and MAO5, one

immediately following the MAO5 lower boundary, and one at the MAO5 midpoint (Figure 3). These were selected to allow the comparison of data from prior to and after the CIE inception, and to allow comparison of sections within the higher moisture availability mesic interval of MAO5 with the winter wet, moisture limited intervals of MAO4 and MAO5 (Figure 3).

Analysis of these samples yielded data with a conservative species composition, showing little taxonomic variation (Figures 5-8). Within each of the four 0.05 m – 0.06 m spaced sample intervals, the normalised palynological data yields a shared pattern of taxon distribution and abundance. All sections display fluctuations in the abundance of pine and swamp cypress pollen (*Pityosporites haplox* and *Inaperturopollenites hiatus*) with increasing frequencies of the Normapolles pollen *Subtriporopollenites anulatus* subsp. *anulatus*. reflecting a shift from higher to lower moisture availability. Although the 0.05 m – 0.06 m sampled intervals are from relatively wetter/cooler and dryer/warmer intervals of MAO4 and MAO5, the lack of any significant compositional change supports an interpretation of plant ecosystem stability and conservatism at sub-centennial scales.

This analysis was performed on intervals in the upper sections of the ~2 ky putative Hallstatt cycles, because they comprise successions of sub-mm laminated mudrocks. The lower intervals of the ~2ky cycles are composed of series of thin fining-upwards deposits (Figure 3), which are probably the lithological equivalent of the wetter-dryer cycles in the laminate palynofloras. Combining the sedimentary cycles with the palynology data from the younger mudrock interval of each ~2 ky cycle suggests a frequency of 9 to 10 cycles per ~2ky, i.e. ~200 y recurrence. Variability at this scale is consistent with solar DeVries/Suess cycles (De Vries, 1958; Suess, 1980, Damon and Sonett, 1991; see also Lüdecke et al., 2015). Although invoking a solar forcing mechanism for these vegetation oscillations is

speculative, the data at least confirm that the palynological data from these intervals is likely recording changes at a tempo comparable to anthropogenic climate forcing.

## **Laminations**

A further data set gathered from 96 consecutive laminations taken at 464.83 m (Figure 3) show similar patterns in taxon frequency changes and associations as recorded in the 0.05 – 0.06 m sampled intervals. Decreasing taxonomic diversity over groups of consecutive laminations are reflected in the standard deviation of the dataset (Figure 9). Boundaries between lamination packages are picked out by an abrupt increase in diversity, and have been used to define oscillations. Variance in the numbers of laminations within each oscillation are in part caused by laboratory constraints on separating the laminations prior to palynological processing, and potentially by depositional or erosional factors. Despite these constraints, spectral analysis of palynomorph density (specimens/g) data indicates a cyclicity with a period of ~12 laminae (10-14 taking into account the bandwidth error, Figure 9).

Within each of these lamination-scale oscillations (Figure 9) the oldest interval is dominated by *Tricolpites cf hians* (Platanaceae) and *Inaperturopollenites hiatus* grading up-section into dominance by *Subtriporopollenites anulatus* subsp *anulatus* through the middle and upper intervals of each cycle. This gradation is reflected in a shift from higher diversity to lower diversity and lower dominance flora, reaching a minimum diversity in the youngest interval of each oscillation. This pattern of species distribution and changes in diversity and dominance reflect short duration transitions between mesic floras and 'savanna' type vegetation of the kind seen in the ~2 ky cycles. Preliminary examination of petrographic sections of the laminations in this section of the core indicate that they are probably

seasonal couplets (Ebinghaus et al., 2017). The distribution of the palynofloras within the cycles identified does not clearly reflect seasonality, potentially due to taphonomic factors and physical difficulties of laminate separation prior to palynological processing. Nevertheless, the spectral analysis does support the possibility that oscillations observed in this series of consecutive laminations are attributable to ~11 y Schwabe solar cycles (e.g. Damon and Sonett, 1991; Figure 8). Evidence supporting the preservation of these cycles in geological archives is rare (e.g. Weedon et al., 2003), and indeed only the lower part of the analysed interval seems to show oscillations at this period (Figure 8). Nevertheless, Ripepe et al. (1991) documented evidence for Schwabe cycles in varve thickness data in the similarly organic-rich lacustrine shale of the Eocene Green River Formation.

#### **Evidence for critical shifts in plant Ecosystems**

The abrupt shift in the composition of the palynofloras at the boundaries between MAO4 and MAO5 and between MAO5 and MAO6 is the most notable feature of the 0.30m spaced palynofloral data set (Figures 3, 4). Change point analysis (Supplementary data 2) of the DCA axis 1 data, alongside plots of mesic to winterwet ratios and the composition of the DCA groups all indicate rapid shifts in floral composition. Winterwet biome taxa are replaced as the dominant group by mesic taxa at 480.9m (MAO 4/MAO 5 boundary) within the 0.30m sample spacing (Figure 4). A second, similarly rapid compositional change is seen at 454.49m (MAO5/MAO6 boundary) where winterwet groups are again replaced as the dominant taxon within 0.30m (Figure 43). Change of this magnitude between samples could infer that this shift in composition took place over ~116 to ~175 y, the average duration of sample spacing in ~2 ky cycles 4.12 and 5.1 respectively (Figures 3,4). The sediments at the base of MAO 5 boundary are poorly sorted turbiditic sandstone deposited as a single event (Figure

3), which, taken together with the presence of putative ~200 y oscillations in the 0.05 m - 0.06 m sample data adjacent to this interval (Figures 5 and 6), supports change in <200 y. While this is an order of magnitude longer than some of the examples of regime shift in the record of modern ecosystems (Reid et al 2015, Capon et al., 2015), elements of floral inertia (Jolley et al., 2015) in the Danian plant ecosystems (rather than the algal systems considered by the aforementioned authors), highlight this as a regime shift event. At the temporal resolution considered here, the response times of individual species to forcing will place a finite limit on the record of palynofloral change. Time taken to reproduce and deposit significant frequencies of pollen/spores to the record may be several decades in mesic woodland, although considerably shorter in shrub/herb dominated savannah. While this inertia would slow the apparent transition from winterwet to mesic communities, any transition from mesic to winterwet communities resulting in plant death would appear more rapid. This is probably illustrated at the ~8 ky oscillation boundaries within MAO5 (at 470.6 m and 461.0 m), where an apparently stepwise transition to a dryer palynoflora is recorded (Figure 3).

Identifying the boundary between MAO4 and MAO5 as a regime raises further questions with regards to evidence for the presence or absence (van Hoof et al., 2008) of ecosystem flickering (Wang et al., 2012) prior to the event. Taking the 0.30 m spaced palynology data, the first axis of the principal components analysis was fitted to a sum of sinusoids line and the residuals expressed as raw and loess smoothed plots (Figure 10). These plots summarise the degree of compositional fluctuation between mesic and winterwet states. Most notably, the amplitude of fluctuation increases in the four ~2 ky (Hallstatt) cycles prior to the MAO4/MAO5 and MAO5/MAO6 boundaries. Compositional fluctuation of this nature is comparable to flickering in modern ecological systems. In the case of the Boltsh crater flora, the onset of flickering may be related to the phase of the precession cycle:

winterwet florae adapted to maximum radiative forcing (Figure 4) become increasingly unstable as forcing decreases. The shorter frequency fluctuations between mesic and winterwet community states may reflect forcing from Hallstatt solar cycles overprinted on the longer term trend. The MAO4/MAO5 boundary for example is inferred to be on at the mid-point between maximum and minimum forcing, resulting in increasing moisture availability and cooler climatic conditions (Figures 4 and 10). Modification of this forcing by solar cycles resulted in increasingly extreme compositional fluctuations in the parent vegetation, prior to reaching a tipping point. On reaching the tipping point, the shift from a winterwet biome to a stable ecological state in a mesic forest biome occurred in <200 y.

## **Uncoupling orbital and solar forcing from hyperthermal impact on vegetation communities**

The Dan-C2 CIE likely represents a massive input of  $^{13}\text{C}$ -depleted carbon into the ocean and atmosphere, making it genetically similar to other CIE records (Gilmour et al., 2013). While a good deal of debate is beginning to focus on the rate of climate change associated with these levels of  $^{13}\text{C}$ -depleted carbon, the high resolution palynofloral data from the Boltys record questions the efficacy of carbon release at the Dan-C2 in driving rapid vegetation community change. From analysis of vegetation community dynamics in this study, it has been possible to identify the impact of orbital and perhaps solar forcing in driving climate change at decadal to centennial scales. However, it is clear that sedimentary depositional system, plant communities, and climate all show slower changes that are correlative with the Dan-C2 isotope excursion (Gilmour et al., 2013, Jolley et al., 2015). The increasing dominance of the thermophilic Normapolles group and the corresponding decline in pteridophyte spores and temperate angiosperm taxa in the CIE Stage 2 supports an

increasingly warm and dry climate (Gilmour et al., 2013; Jolley et al., 2015). The dislocation between the changes in palynofloras consequent on orbital and solar forcing, and the change consequent on an overall climate warming from the hyperthermal event is one of tempo. This is illustrated by the high resolution  $\delta^{13}\text{C}$  record presented here (Figure 3), using 0.30 m spaced samples. Although exhibiting significant fluctuations, the 1 m sample spaced data of Gilmour et al., (2013) and the 0.30 m spaced loess smoothed C-isotope data are similar and show an increasingly negative trend over the period spanning the winterwet phase MAO4 to winterwet phase MAO 5 of  $\sim -3\text{‰}$ . This change is reflected in a minor shift between the warmer/dry phase of MAO4 and the warmer/dry phase of MAO5 recorded by the DCA axes plot (Figure 3). A shift is also apparent between the mesic phase of MAO5 and mesic phase of MAO6 (6.2% increase in mean DCA Axis I value) and the winterwet phases of MAO4 and MAO5 (7.8% increase in mean DCA Axis I value). These shifts indicate an increasingly dryer and warmer environment across the CIE inception on a multi-centennial scale. The absence of a rapid negative  $\delta^{13}\text{C}$  excursion within these data suggests that, at least in the case of Dan-C2, the increase in atmospheric  $\text{CO}_2$  was perhaps a result of a prolonged buildup rather than a single rapid event.

## Conclusions

Situated near to the northern shores of the Tethyan Ocean, the Boltysh crater lake formed at a paleolatitude of around  $30^\circ\text{N}$  (Figure 1). Alternation between mesic and winterwet biomes has been recorded at frequencies consistent with both orbital and solar forcing, with a longer-term overprint of the greenhouse warming impact of the Dan-C2 event. Although the mechanistic link between solar forcing and vegetation remains unclear, perhaps the two most remarkable components of the Boltysh record are the evidence for a

340 'sluggish' CIE inception, and the rapidity of biome regime shift at MAO/~21ky precession  
341 cycle boundaries.

342 Evidence for a gradual onset to the Dan-C2 hyperthermal event, and rapid responses to  
343 orbital and sub-orbital forcing indicates that control over the savannah – mesic transition  
344 was perhaps derived from the poleward shift of Hadley cell margins. Global warming under  
345 greenhouse conditions would be anticipated to bring about a northern expansion of Hadley  
346 cells and the down current of stable, dry air migrating north across the study area  
347 (Hasegawa et al, 2012; Davis et al., 2016). This would have led to the northern expansion of  
348 the savannah, or winterwet biome on the northern shores of Tethys, driving the mesic  
349 vegetation belt further to the north. From the repeated alternations between mesic and  
350 winterwet biome dominance, it follows that orbital and perhaps solar forcing operated  
351 control over the poleward extent of the Hadley cell. Comparable forcing was operated at a  
352 slower tempo by the warming and subsequent cooling of the Dan-C2 hyperthermal.

353 In contrast to the suggested collapse of Hadley cells in response to the mid Cretaceous  
354 supergreenhouse (Hasegawa et al. 2012), the Boltysh record indicates that the Danian  
355 climate retained a subtropical jet zone. Although rapid regime shift happened at the  
356 boundary of MAO's/~21ky cycles there is no evidence to support sudden climate change at  
357 these points. Rather, the evidence indicates that when vegetation biomes became  
358 unbalanced with respect to climatic change as a consequence of orbital forcing, species  
359 were pushed to the limit of their ecological range. The Boltysh vegetation communities in  
360 this state were susceptible to collapse, leading to rapid plant community regime shift.

361 Evidence from the Boltysh palynological and carbon isotope record does not support a  
362 rapid inception for the Dan-C2 CIE. The high-resolution record (Figures 2, 3) shows a  
363 decline of ~4 ppm over ~21 ky. Although this seemingly eliminates this CIE as a deep time



proxy record against which to predict the impact of anthropogenic climate change, the impact of orbital and solar forcing on vegetation community dynamics highlights a record of repeated climate warming over decadal and longer scales.

With future modelled predictions of climate change indicating a northward expansion of subtropical arid climates away from the equatorial zone (Davis et al., 2016), the Boltysh record provides insight into associated vegetation dynamics in a comparable deep time system. Coincidence of solar and orbital forcing with elevated anthropogenic CO<sub>2</sub> have the potential to force regime shift in environmentally stressed plant ecosystems on a decadal scale with consequent societal impacts.

## **Acknowledgements**

The drilling of the Boltysh crater was funded by Natural Environment Research Council (NERC) grant NE/D005043/1. The authors would like to thank Prof. R.A. Spicer for his helpful comments on a draft manuscript and two anonymous referees for their constructive comments.

380

381

## References

- 382 Abels, H.A., Clyde, W.C., Gingerich, P.D., Hilgen, F.J., Bowen, G.J. & Lourens, L.J. 2012.  
383 Terrestrial carbon isotope excursions and biotic change during Palaeogene hyperthermals. *Nature*  
384 *Geoscience* 5, 326–329, doi:10.1038/ngeo1427
- 385 Alexander, K, Meissner, K.J. & Bralower, T.J. 2015. Sudden spreading of corrosive bottom  
386 water during the Palaeocene–Eocene Thermal Maximum. *Nature Geoscience* 8,458–461.  
387 doi:10.1038/ngeo2430.
- 388 Capon, S.J., Lynch, A.J.J., Bond, N., Chessman, B.C., Davis, J., Davidson, N., Finlayson, M.,  
389 Gell, P.A., Hohnberg, D., Humphrey, C., Kingsford, R.T., Nielsen, D., Thomson, J.R., Ward,  
390 K. & Mac Nally, R. 2015. Regime shifts, thresholds and multiple stable states in freshwater  
391 ecosystems; a critical appraisal of the evidence. *Science of the Total Environment* 534, 122–130
- 392 Coccioni, R., Frontalini, F., Bancala, G., Fornaciari, E., Jovane, L., Sprovieri, M., 2010. The  
393 Dan-C2 hyperthermal event at Gubbio (Italy): Global implications, environmental effects,  
394 and cause(s). *Earth and Planetary Science Letters* **297**, 298–305.
- 395 Cui, Y. Kump, L. Ridgwell, A., Deifendorf, A & Junium, C.K. 2010 A high resolution record  
396 from Svalbard of Carbon Release during the Paleocene – Eocene Thermal Maximum. *Journal*  
397 *of Earth Science* 21, 190-193
- 398 Damon, P.E., and Sonnett, C.P., 1991, Solar and terrestrial components of the atmospheric  
399 <sup>14</sup>C variation spectrum, in Sonnett, C.P., Giampapa, M.S., and Matthews, M.S., eds., *The sun*  
400 *in time*: Tucson, Ariz., The University of Arizona Press, p. 360–388.

401 Daly, R. & Jolley D.W., 2015. What was the nature and role of Normapolles angiosperms? A  
 402 case study from the earliest Cenozoic of Eastern Europe. *Palaeogeography, Palaeoclimatology,*  
 403 *Palaeoecology* 418, 141-149.

404 Davis N.A., Seidel, D.J., Birner, T., Davis, S.M. & Tilmes, S. 2016.Changes in the width of the  
 405 tropical belt due to simple radiative forcing changes in the GeoMIP simulations. *Atmospheric*  
 406 *Chemistry and Physics* 16, 10083–10095.

407 De Vries, H. 1958. Variation in concentration of radiocarbon with time and location on  
 408 Earth. *Koninkl Ned Akad Wetenschappen, Proc B* 61, 94-102.

409 Dinarès-Turell, J., Westerhold, T., Pujalte, V., Röhl, U. & Kroon, D. 2014. Astronomical  
 410 calibration of the Danian stage (Early Paleocene) revisited: Settling chronologies of  
 411 sedimentary records across the Atlantic and Pacific Oceans, *Earth Planetary Science Letters*,  
 412 405, 119-131.

413 Ebinghaus, A., Jolley, D. W., Andrews, S. & Kemp, D. B. et al. 2017. Lake sedimentological  
 414 and ecological response to hyperthermals: Boltysh impact crater, Ukraine. *Sedimentology* in  
 415 press.

416 Gallagher, K., Bodin, T. Sambridge, M., Weiss, D., Kylander, M. & Large, D., 2011. Inference  
 417 of abrupt changes in noisy geochemical records using transdimensional  
 418 changepoint models. *Earth and Planetary Science Letters* 311 (2011) 182–194

419 Gilmour, I., Jolley, D.W., Kemp, D.B., Kelley, S.P., Gilmour, M., Daly, R. & Widdowson, M  
 420 2014. The early Danian hyperthermal event at Boltysh (Ukraine): Relation to Cretaceous –  
 421 Paleogene boundary events. In: Keller, G. & Kerr, A.C. (eds.) *Volcanism, Impacts and Mass*  
 422 *Extinctions: Causes and Effects*. Geological Society of America Special Paper 505. Doi  
 423 10.1130/2014.2505(06).

424 Gilmour, I., Gilmour, M., Jolley, D., Kelley, S. Kemp, D. Daly., R. & Watson, J. 2013. A high  
 425 resolution nonmarine record of an early Danian hyperthermal event, Boltysh crater, Ukraine.  
 426 *Geology* **41**, 783-786.

427 Hammer, Ø., Harper, D.A.T., & P. D. Ryan, 2001. PAST: Paleontological Statistics software  
 428 Package for Education and Data Analysis. *Palaeontologia Electronica* 4(1), 9pp.

429 Hasegawa, H., Tada, R., Jiang, X., Suganuma, Y., Imsamut, S., Charusiri, P., Ichinnorov, N. &  
 430 Khand, Y., 2012. Drastic shrinking of the Hadley circulation during the mid-Cretaceous  
 431 Supergreenhouse. *Climates of the Past* 8, 1323–1337. doi:10.5194/cp-8-1323-2012

432 Herbert, T. D., 1994. Reading orbital signals distorted by sedimentation: Models and  
 433 examples, in DeBoer, P. L. & Smith, D. G. (eds), *Orbital Forcing and Cyclic Sequences*,  
 434 Special Publication 19 of the IAS (International Association of Sedimentologists Series),  
 435 576pp, Wiley-Blackwell, Oxford, U. K.

436 Hesselbo S. & Pieńkowski G. 2011. Stepwise atmospheric carbon-isotope excursion during  
 437 the Toarcian Oceanic Anoxic Event (Early Jurassic Polish Basin). *Earth & Planetary Science*  
 438 *Letters* **301**, 365-372.

439 Hesselbo, S.P., Gröcke, D.R., Jenkyns, H.C., Bjerrum, C.J., Farrimond, P., Morgans Bell, H.S.  
 440 & Green, O.R. 2000. Massive dissociation of gas hydrate during a Jurassic oceanic anoxic  
 441 event *Nature* 406, 392-395 doi:10.1038/35019044.

442 Jolley, D.W., Gilmour, I., Gilmour, M., Kemp, D.B. & Kelley, S.P. 2015. Long-term resilience  
 443 decline in plant ecosystems across the Danian Dan-C2 hyperthermal event, Boltysh crater,  
 444 Ukraine. *Journal of the Geological Society, London*, 172, 491-498.

445 Jolley, D.W., Daly, R.J., Gilmour, I. & Kelley, S.P. 2013. Climatic oscillations stall vegetation  
 446 recovery from K/Pg event devastation. *Journal of the Geological Society of London* **170**, 477-  
 447 482.

448 Jolley, D.W., Gilmour I, Gurov, E., Kelley, S.P. & Watson, J.S. 2010. Two large meteorite  
 449 impacts at the Cretaceous - Paleogene boundary. *Geology* **38**, 835-838.

450 Kemp, D.B., Coe, A.L., Cohen, A.S. & Schwark, L. 2005. Astronomical pacing of methane  
 451 release in the Early Jurassic period. *Nature* **437**, 396-399.

452 Kern, A.K., Harzhauser, M., Piller, W.E., Mandic, O. & Soliman, A. 2012. Strong evidence for  
 453 the influence of solar cycles on a Late Miocene lake system revealed by biotic and abiotic  
 454 proxies. *Palaeogeography, Palaeoclimatology, Palaeoecology*, 329–330, 124–136.

455 Kirtland Turner, S & Ridgwell, A. 2013. Recovering the true size of an Eocene hyperthermal  
 456 from the marine sedimentary record. *Paleoceanography* **28**, 700–712,  
 457 doi:10.1002/2013PA002541

458 Kovach, W. L. 2002. *MVSP – A Multivariate Statistical Package for Windows ver 3.1*. Kovach  
 459 Computing Services, Pentraeth, Wales, UK.

460 Lenz, O.K., Wilde, V. & Riegel, W. 2016. ENSO- and solar-driven sub-Milankovitch cyclicity  
 461 in the Palaeogene greenhouse world; high-resolution pollen records from Eocene Lake  
 462 Messel, Germany. *Journal of the Geological Society*, **174**, 110-128, doi:10.1144/jgs2016-046.

463 Lüdecke H.J., Weiss, C.O. & Hempelmann, A. 2015. Paleoclimate forcing by the solar  
 464 De Vries/Suess cycle. *Climate of the Past, Discussion* **11**, 279–305.

465 Lunt, D.J., Ridgwell, A., Sluijs, A., Zachos, J., Hunter, S. & Haywood, A. 2011. A model for orbital  
 466 pacing of methane hydrate destabilization during the Palaeogene. *Nature Geoscience* **4**, 775–778.  
 467 doi:10.1038/ngeo1266

468 Mehay, S., Keller, C.E., Bernasconi, S.M., Weissert, H., Erba, E., Bottini, C. & Hochuli, P.A.,  
 469 2009. A volcanic CO<sub>2</sub> pulse triggered the Cretaceous Oceanic Anoxic Event 1a and a  
 470 biocalcification crisis. *Geology*, **37**, 819-822.

471 Quillévéré F., Norris, R.D., Kroon, D. & Wilson, P.A. 2008. Transient ocean warming and  
 472 shifts in carbon reservoirs during the early Danian. *Earth and Planetary Science Letters* **265**,  
 473 600–615.

474 Reid, P.C. Hari, R.E., Beaugrand, G., Livingstone D.M., Marty, C., Straile, D., Barichivich, J.,  
 475 Goberville, E., Adrian, R., Aono, Y., Brown, R., Foster, J., Groisman, P., Elaoucet, P., Hsu,  
 476 H., Kirby, R., Knight, J., Kraberg, A., Li, J., Lo, T-T., Myneni, R.B., North, R., Pounds, J.A.,  
 477 Sparks, T., Stubi, R., Tiab, Y., Wiltshire K.H., Xiao, D. & Zhu, Z., 2015. Global impacts of the  
 478 1980s regime shift. *Global Change Biology*, doi: 10.1111/gcb.13106

479 Ripepe, M., Roberts, L.T. & Fischer, A.G., 1991. Enso and sunspot cycles in varved Eocene  
 480 oil shales from image analysis. *Journal of Sedimentary Petrology*, 61, 1155-1163.

481 Scotese, C.R., 2014. Atlas of Late Cretaceous Maps. PALEOMAP Atlas for ArcGIS, volume  
 482 2, The 630 Cretaceous, Maps 16-22, Mollweide Projection, Evanston, IL.

483 Sprain, C.J., Renne I, P.R., Wilson, G.P. & Clemens, W.A. 2015. High-resolution  
 484 chronostratigraphy of the terrestrial Cretaceous-Paleogene transition and recovery interval  
 485 in the Hell Creek region, Montana. *Geological Society America Bulletin* 127, 393–409; doi:  
 486 10.1130/B31076.1

487 Suess, H. E., 1980. The radiocarbon record in tree rings of the last 8000 years. *Radiocarbon*,  
 488 22, 200–209.

489 Van Hoof, T.B, Wagner-Cremer, F., Kuershner, W.M. & Vischer, H. 2008. A role for  
 490 atmospheric CO<sub>2</sub> in pre industrial climate forcing. *Proceedings of the National Academy of*  
 491 *Sciences* 105 (41), 15815-15818.

492 Wang, R., Dearing, J.A., Langdon, P.G., Zhang, E., Yang, X., Dakos, V. & Scheffer, M. 2012.  
 493 Flickering gives early warning signals of a critical transition to a eutrophic lake state. *Nature*  
 494 **492**, 419-422.

Weedon, G. P., 2003. Time-Series Analysis and Cyclostratigraphy, 259 pp., Cambridge Univ. Press, Cambridge, U. K., doi:10.1017/CBO9780511535482.

Wright, James D.; Schaller, Morgan F.R, 2014. Reply to Pearson and Nicholas, Stassen et al., and Zeebe et al.: Teasing out the missing piece of the PETM puzzle. *Proceedings of the National Academy of Science of the United States of America* 111 (12), E1068-E1071.

Zeebe, R.E., Ridgwell, A. & Zachos, J.C. 2016. Anthropogenic carbon release rate unprecedented during the past 66 million years *Nature Geoscience* 9, 325–329, doi:10.1038/ngeo2681.

Zeebe, R. E. Dickens, G. R. Ridgwell, A., Sluijs, A. & Thomas, E., 2014. Onset of carbon isotope excursion at the Paleocene-Eocene thermal maximum took millennia, not 13 years. *Proceedings of the National Academy of Sciences of the United States of America* 111(12), E1062 – E1063.

Zeebe, R.E. & Zachos, J.C., 2013. Long-term legacy of massive carbon input to the Earth system: Anthropocene versus Eocene. *Philosophical Transactions Royal Society A* 371, 20120006. doi.org/10.1098/rsta.2012.

## Figure Captions

### Figure 1

Latest Cretaceous palaeogeographical map of Europe showing the location of the Boltysh impact crater (red circle) at the southern margin of the Fennoscandian landmass on the margins of the Tethyan Ocean (modified from Scotese, 2014).

### Figure 2

Stratigraphical framework for the Boltysh 42/11 cored borehole 230m - 581m. The Boltysh bulk organic matter  $\delta^{13}\text{C}$  record (Gilmour et al., 2013) is compared to bulk carbonate  $\delta^{13}\text{C}$  records from the composite record from a) Zumaia, Spain and ODP hole 1262 South Atlantic (Dinares-Turell et al., 2014) and b) to bulk carbonate  $\delta^{13}\text{C}$  and  $\delta^{18}\text{O}$  records from ODP 1049C, North Atlantic (Quillévéré et al., 2008). The vertical scale for the shorter marine sections is consistent, but because of space constraints, the vertical scale of c) Boltysh 42/11 is reduced by 80%. The position of the K/Pg boundary is at the base of the plotted data for all three sections, while the C29r/C29n boundary is shown for Zumaia and Boltysh. Identification of 'e-bundles' in C29r at Zumaia by Dinares-Turell et al (2014) provides an estimated duration of 200-300ky for this interval. Sequence analysis of moisture availability oscillations (MAO's) in the Boltysh palynofloral record by Jolley et al (2015), and of bulk organic matter  $\delta^{13}\text{C}$  (Gilmour et al., 2013) identifies up to 11x21ky cycles within the post K/Pg boundary interval of C29r. Isotopic dates for ashes at the K/Pg boundary ( $66.043 \pm 0.043$ ) and the base of C29n ( $65.832 \pm 0.036$ , Sprain et al., 2015) indicate a ~211ky interval which is within errors of the duration derived from the MAO cycles of 231ky.



Figure 3

Plant community ecology cyclicity across the Dan-C2 hyperthermal excursion inception 490m – 452m 42/11 borehole. Sampled at 0.3m intervals, the stratigraphical plots of DCA derived groups (see supplementary data 1) show the influxes of mesic groups at the base of each ~2ky cycle (horizontal dashed lines) and the rapid switch from savanna to mesic vegetation community dominance at the boundaries between MAO 4/5 and MAO5/6 (bold horizontal dashed lines). This orbital and possible solar cyclicity is reflected in the Axis 1 DCA stratigraphical plot (bold line is loess smoothed) and the power spectrum of linearly interpolated DCA Axis 2 data. Spectrum calculated using multi-taper algorithm ( $2\pi$ ) with data linearly detrended and interpolated prior to analysis. Confidence levels (CL) set based on least square fitting of a first order autoregressive (AR1) model to the raw spectrum following methods outlined in Weedon (2003). Spectral peaks exceeding the 99% confidence level at ~1 and ~1.6 cycles per metre are unlikely to be robust since these cycles are each defined by <4 data points (e.g. Herbert, 1994). Filtering conducted using a Gaussian bandwidth filter centred on frequency of 0.39. Note that on the left, the cooler, higher moisture availability intervals of both the ~21ky and ~2ky cycles are shaded blue, passing up into yellow/orange dryer and warmer phases. The position of 0.05m-0.06m spaced sample intervals (see Figures 5-8) and consecutively sampled sub-mm laminations are marked in grey on the left.

Figure 4

DCA axis 1 and DCA ecological group data plotted on a chronstratigraphical axis. This is based on a linear extrapolation of the ~2ky cycles, labelled in grey on the left.

Note that the time spacing between 0.3m samples increases in the later, dryer intervals of the ~21ky MAO's reflecting a drop in sedimentation rate in the crater lake. Note the rapid shift from savanna to mesic community dominance at the lower boundaries of MAO5 and MAO6. The synthetic forcing plot on the left of the diagram shows the hypothesised intensity of forcing from the ~21ky precession cycles overlain by ~2ky (hypothetical Hallstatt) cycles. An alternative plot showing the additional forcing potential from the Dan-C2 hyperthermal is shown in red/pink. It is noteworthy that the late stage, savanna dominated floras of MAO4 and MAO5 occur during a period of increasing moisture availability, creating environmental stress for the dry adapted plant ecosystem.

#### Figure 5

Stratigraphical plot of the dominant palynofloral elements in the 0.05m spaced data set from 484.44m to 483m. The cyclic changes to *Subtriporopollentites anulatus* subsp. *anulatus* dominance in the data set are highlighted with dashed lines. This taxon is a Normapolles group pollen, probably derived from scrub like plants. Because these plants mature relatively rapidly, this may account for the sensitivity evident in the distribution of this taxon in comparison to those derived from what are probably larger arborescent taxa (e.g. *Inaperturopollenites hiatus* derived from Cupressaceae).

#### Figure 6

Stratigraphical plot of the dominant palynofloral elements in the 0.05m spaced data set from 476.4m – 475.8m. Horizontal dashed lines denote boundaries between influxes of *Subtriporopollenites anulausl* subsp. *anulatus*.

#### Figure 7

Stratigraphical plot of the dominant palynofloral elements in the 0.05m spaced data set from 471.95m – 471.1m. Horizontal dashed lines denote boundaries between influxes of *Subtriporopollenites anulaus* subsp. *anulatus*.

#### Figure 8

Stratigraphical plot of the dominant palynofloral elements in the 0.05m spaced data set from 461.65m – 460.0m. Horizontal dashed lines denote boundaries between influxes of *Subtriporopollenites anulaus* subsp. *anulatus*.

#### Figure 9

Stratigraphical frequency plot of the palynofloras from 96 consecutive laminations at 464.83m. The apparent sensitivity to environmental change implied by the distribution pattern of the platanaceous pollen *Tricolpites* cf. *hians* indicates that the parent plant was adapted to rapid reproduction, and may have been of scrub or herb physiognomy. The shift to dominance of this taxon in the upper part of the succession is however, probably taphonomic. The horizontal dashed lines mark boundaries between cycles in the data defined by standard deviation of the whole data set. These are supported by a power spectrum of lamina density data showing a clear peak at a period of ~12 laminae. Filtering shows this oscillation is only strong in the lower part of the analysed interval. Filtering was conducted using a Gaussian bandwidth filter centred at the same frequency (i.e. 0.084 cycles per lamina, 0.05 bandwidth). Spectrum was calculated using multi-taper algorithm ( $2\pi$ ) with data linearly detrended prior to analysis. Confidence levels (CL) were set based on least square fitting of a first order autoregressive (AR1) model to the raw spectrum following methods outlined in Weedon (2003).

#### Figure 10

Plot of residuals from a sum of sinusoids line fitted to the DCA axis I data shown in Figure 3. The lithological log is as Figure 3. The bold orange line is the loess smoothed plot of the residuals, and shows a close similarity to the mesic to savanna compositional variation that defines the potential Hallstatt cycles with a period of ~2ky. Note the increase in amplitude of the fluctuations with proximity to the MAO4-MAO5 and MAO5-MAO6 boundaries.

#### **Jolley et al Supplementary data figure captions**

Supplementary data 1: Plot of axis 1 and 2 of the detrended correspondence analysis of the 30cms sample spaced data set between 452m and 489m, borehole 42/11, Boltysh meteorite crater, Ukraine.

Supplementary data 2: Changepoint analysis of the 30cms sample spaced data borehole 42/11, Boltysh crater Ukraine using the approach and software of Gallagher et al. (2011).

Supplementary data 3: Photographs of the 42/11 core: a) 462.2m – 457.7m, b) 466.6m – 462.2m.

Supplementary data 4: Palynological frequency data for DCA groups in the 30cms spaced data set

Figure 1

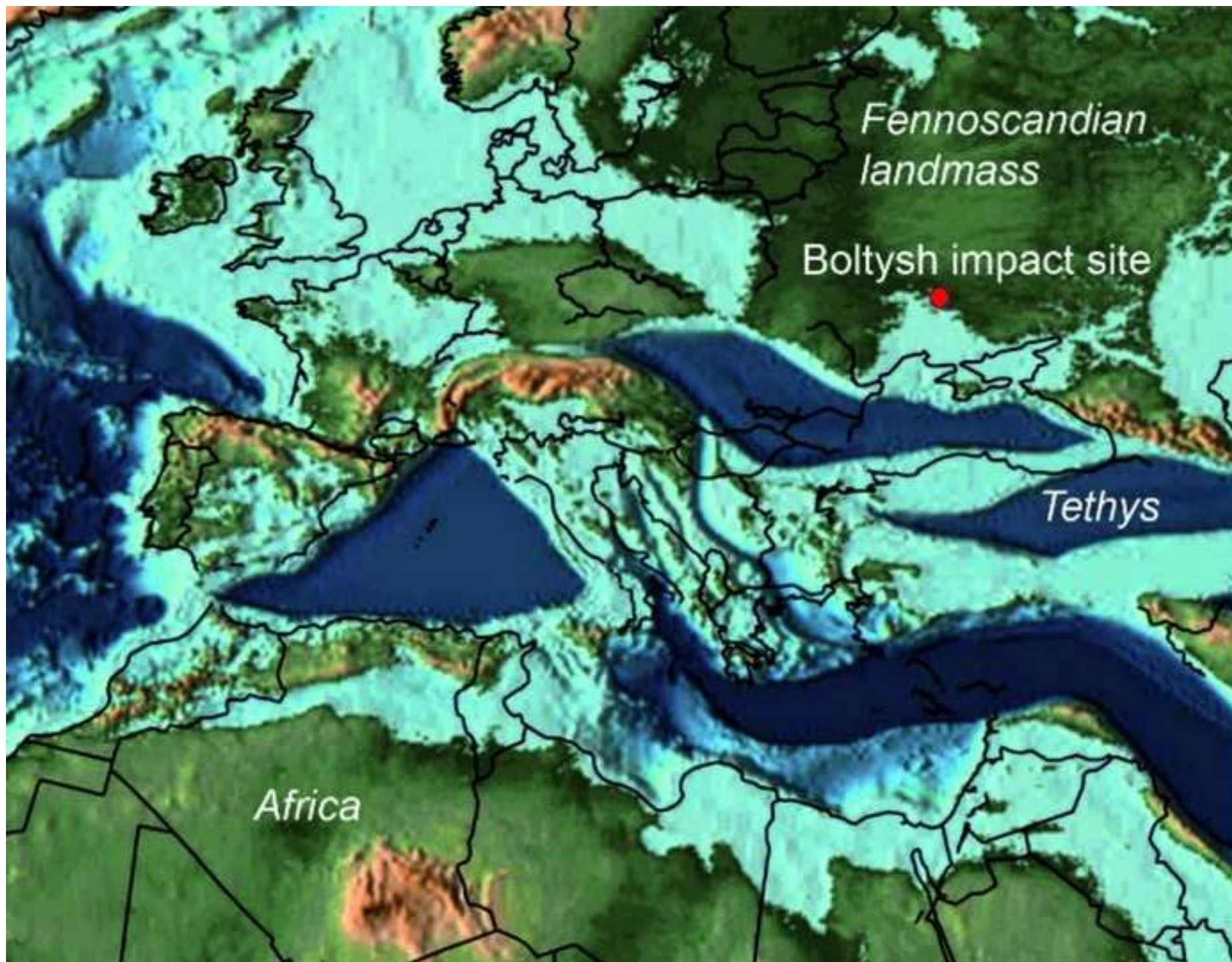




Figure 2

[Click here to download Figure Jolley et al Boltys Fig 2.jpg](#)

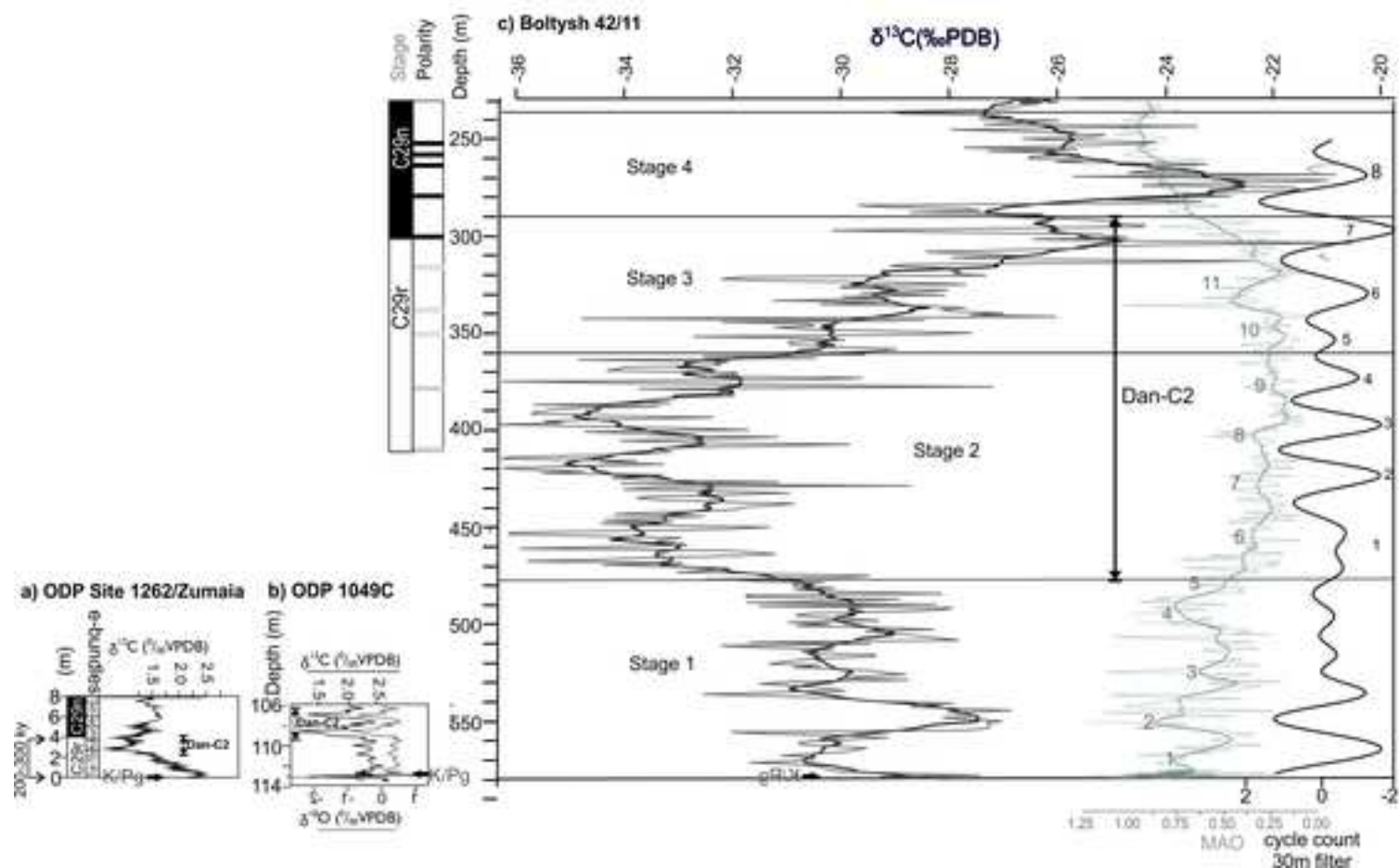
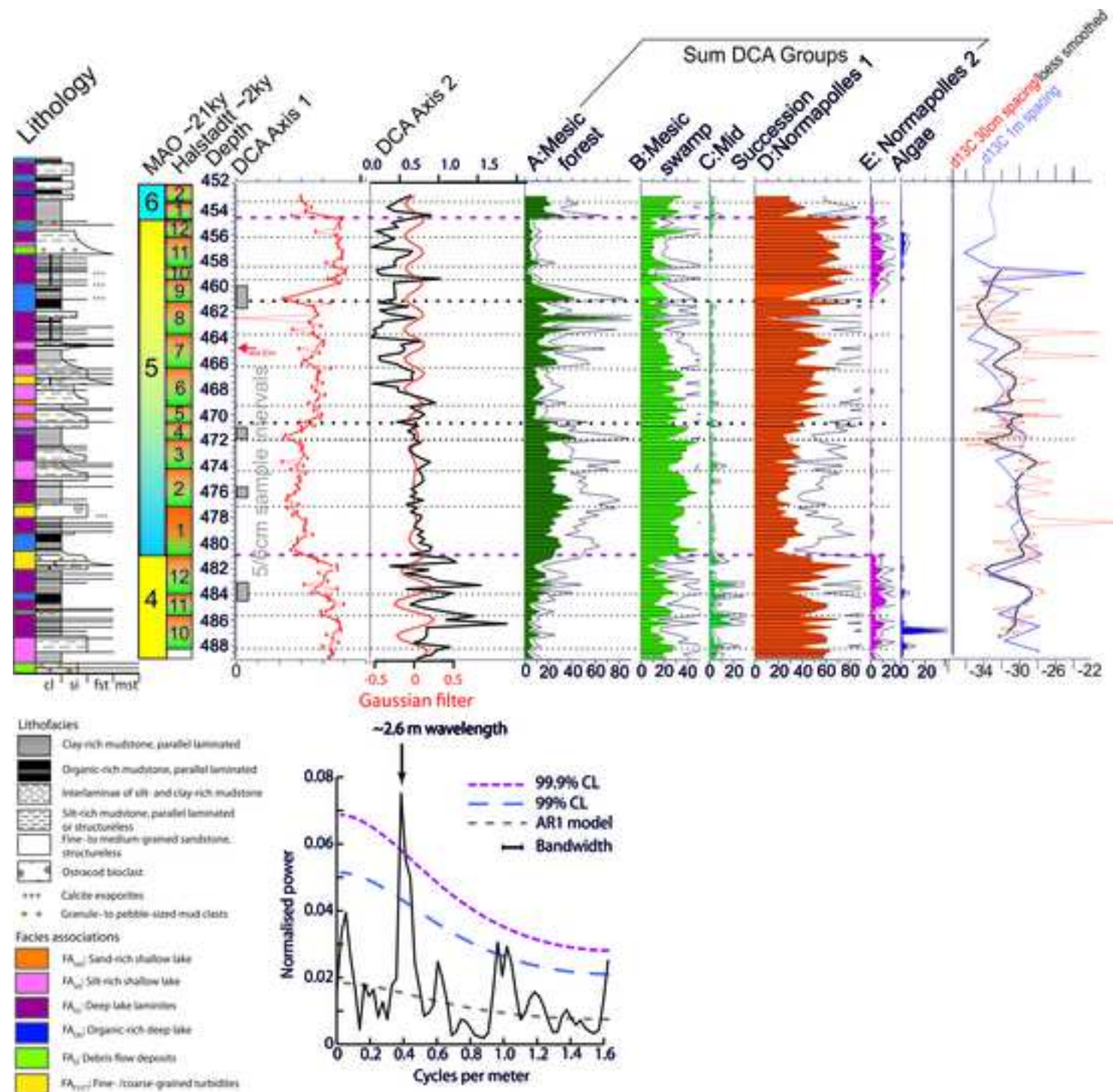
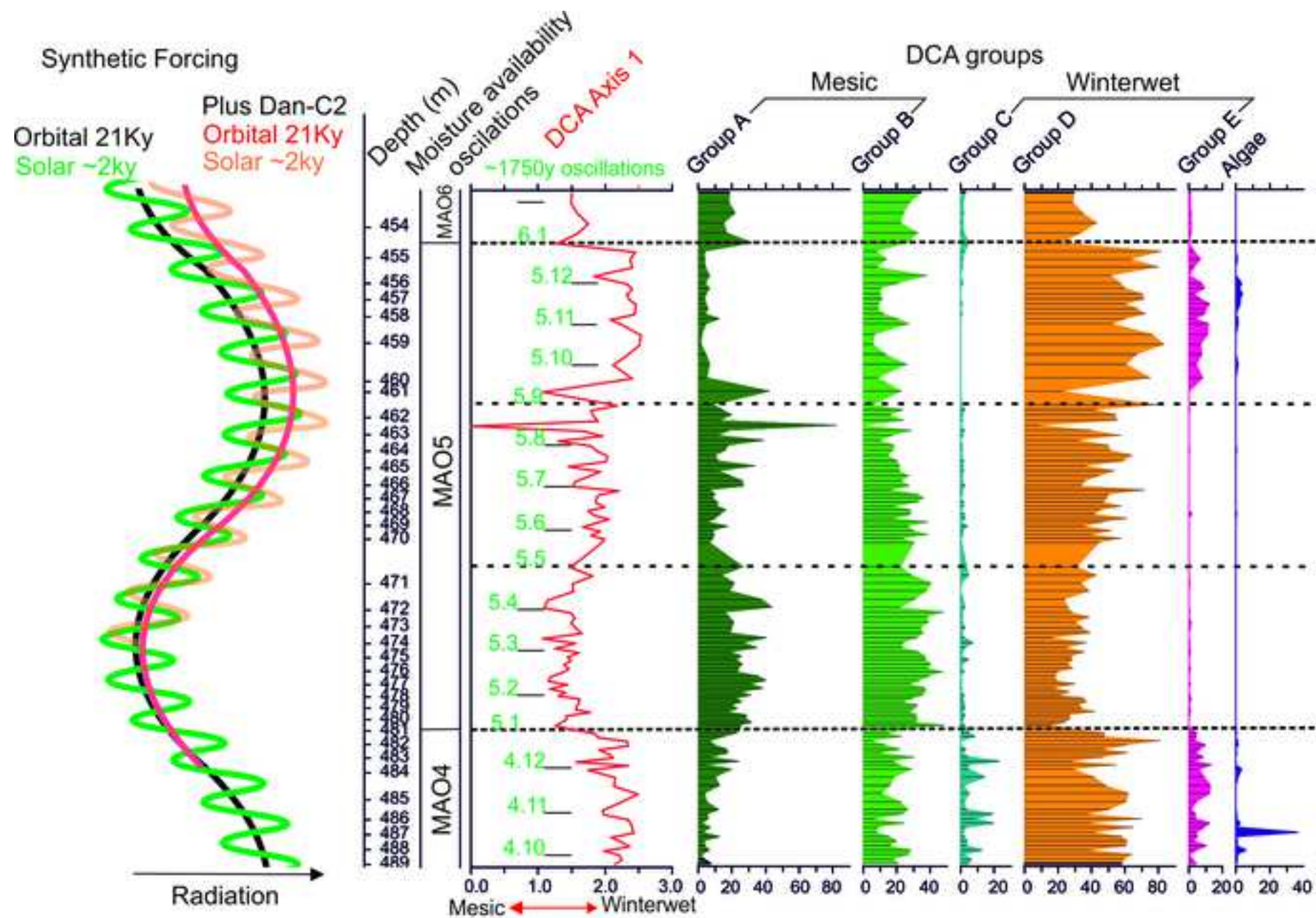


Figure 3

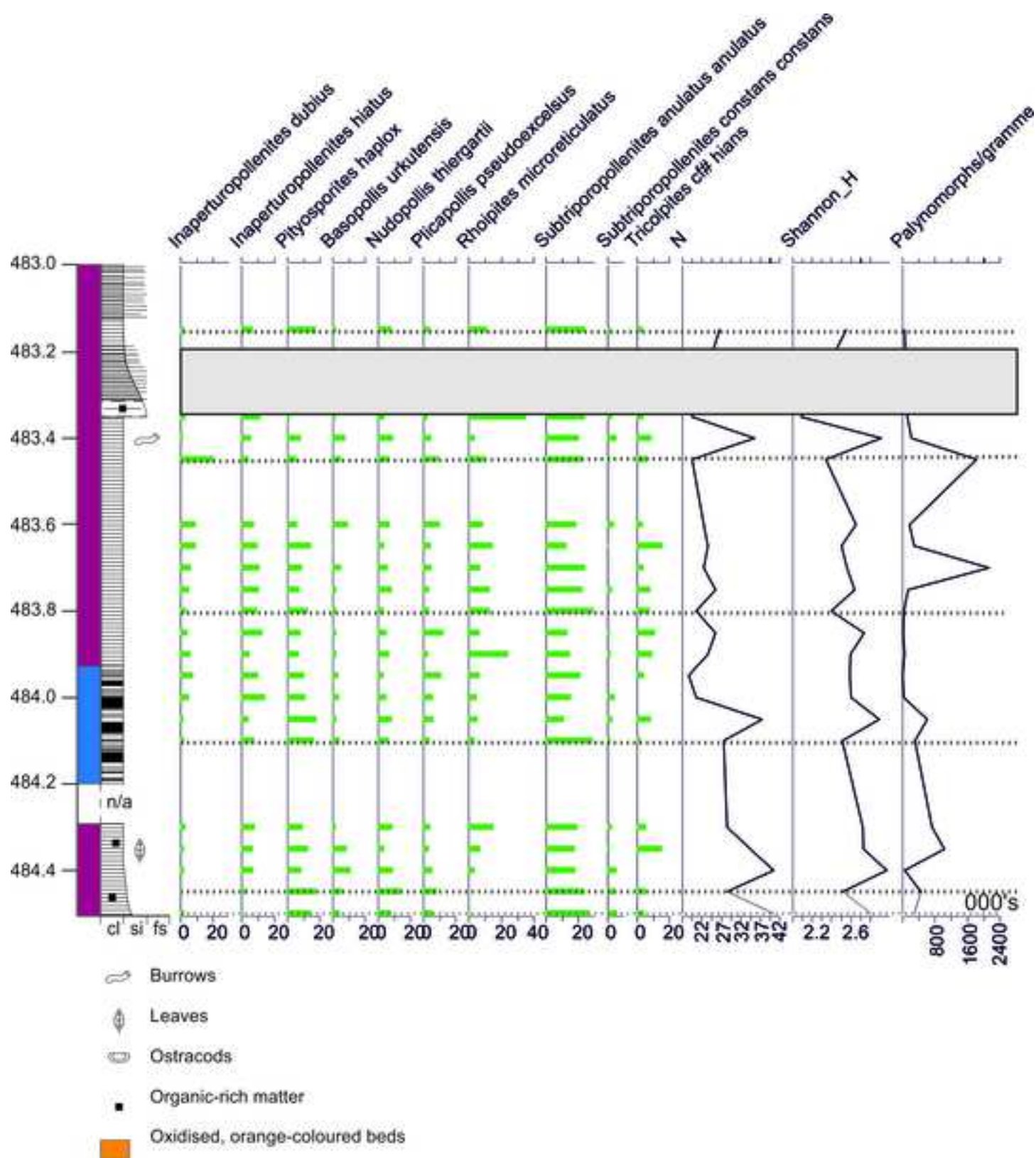


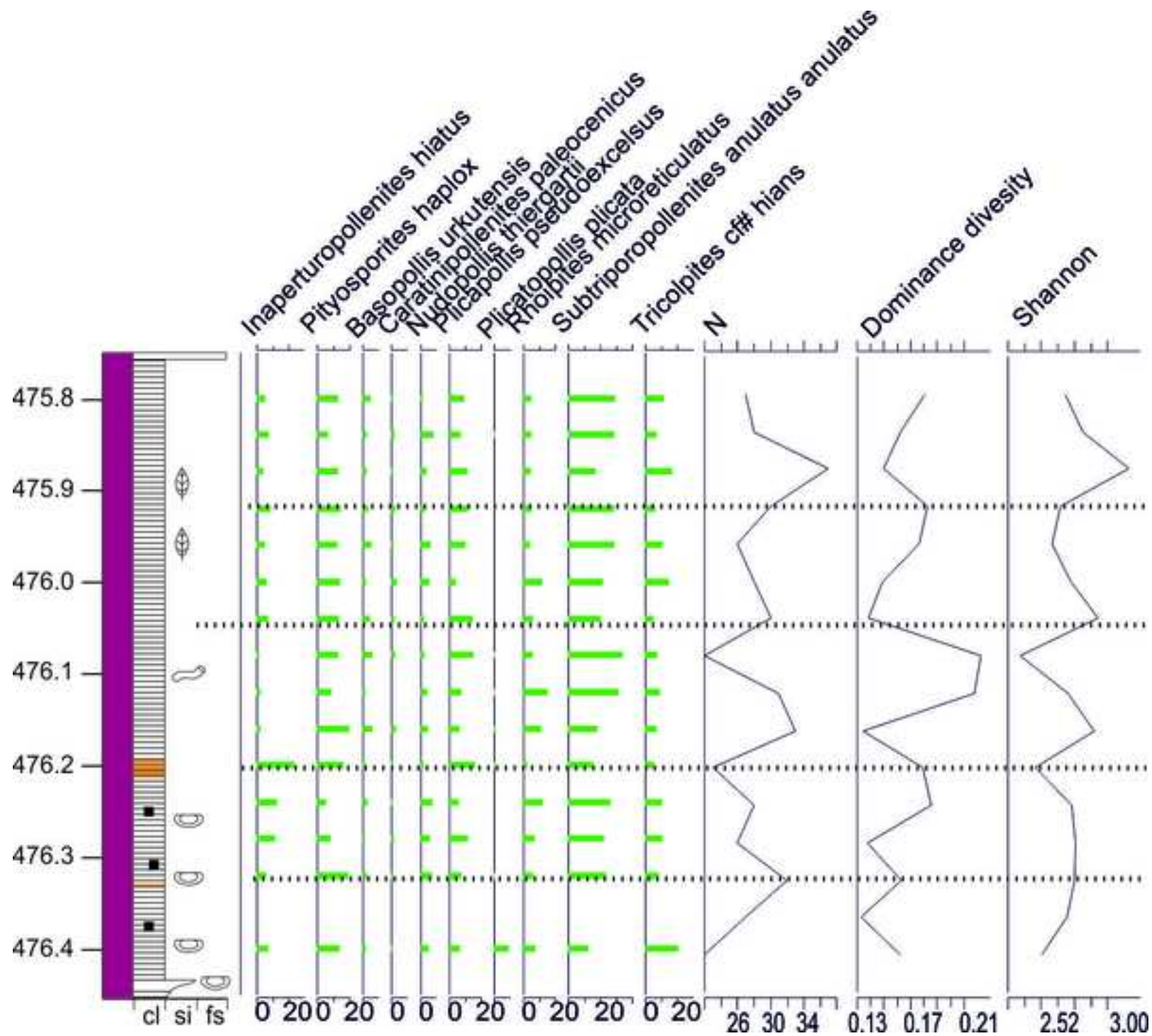
Figure





[Click here to download Figure Jolley et al Boltysch Fig 5.jpg](#) 

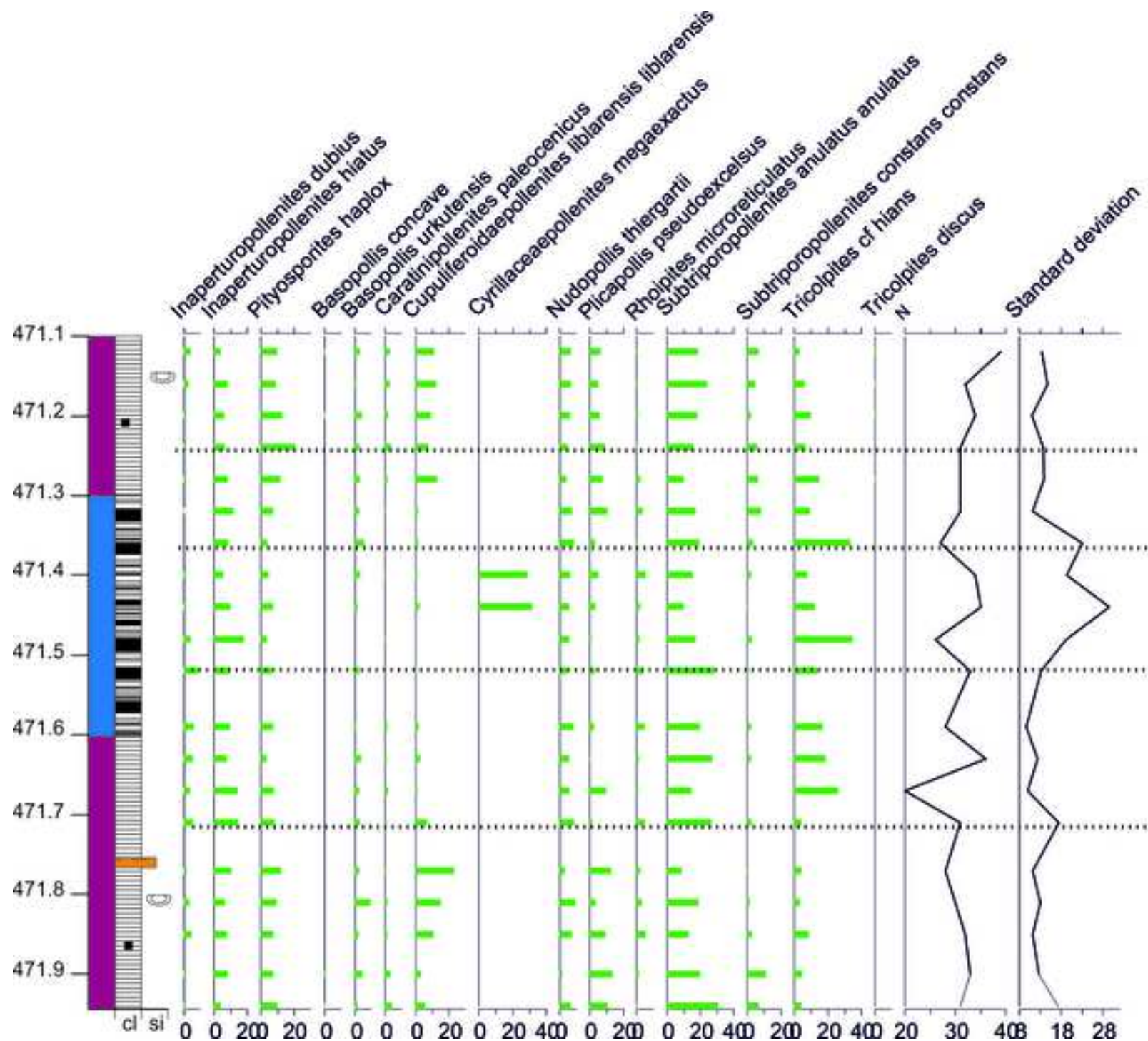




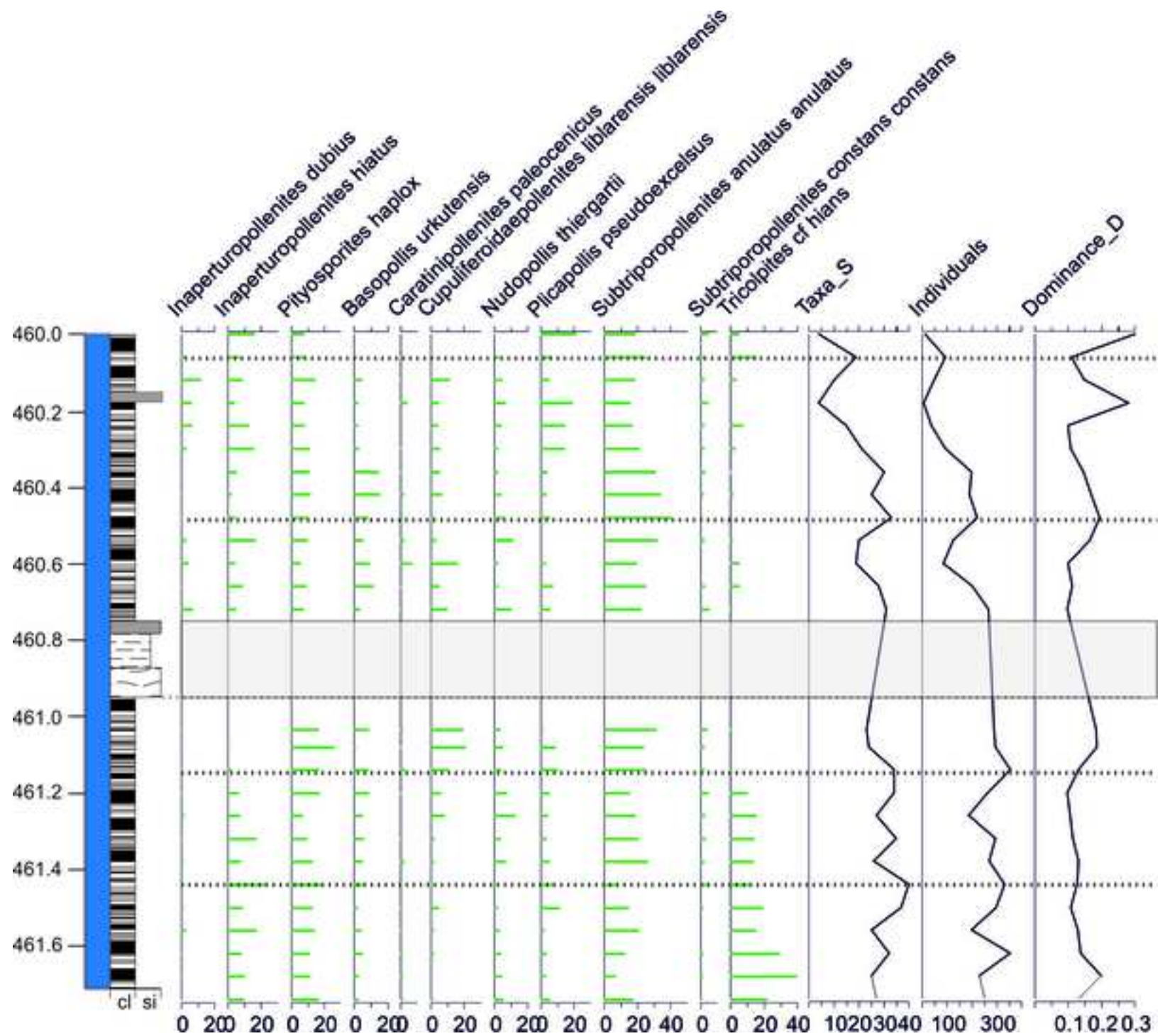


Figure

[Click here to download Figure Jolley et al Boltys Fig 7.jpg](#)

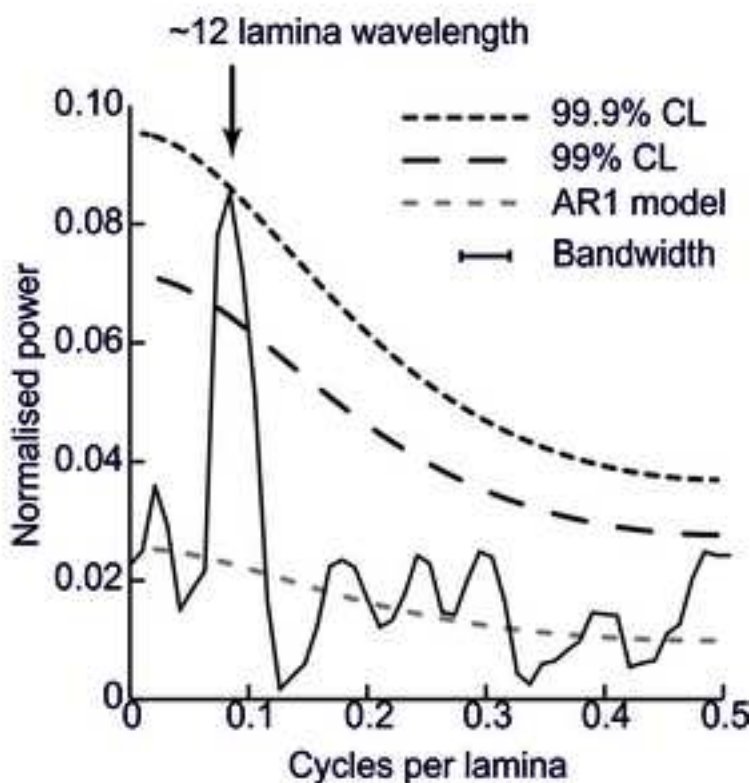
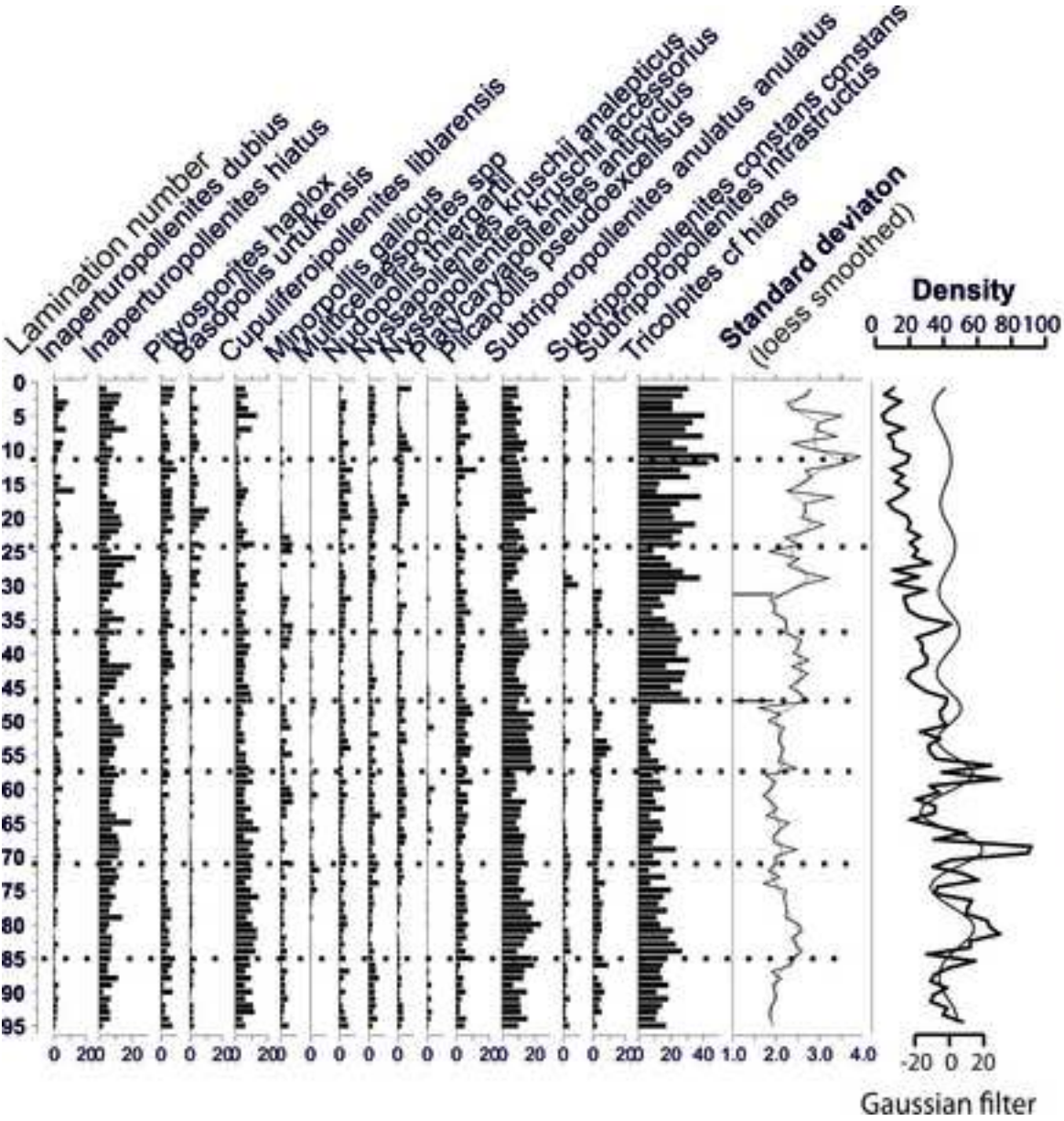


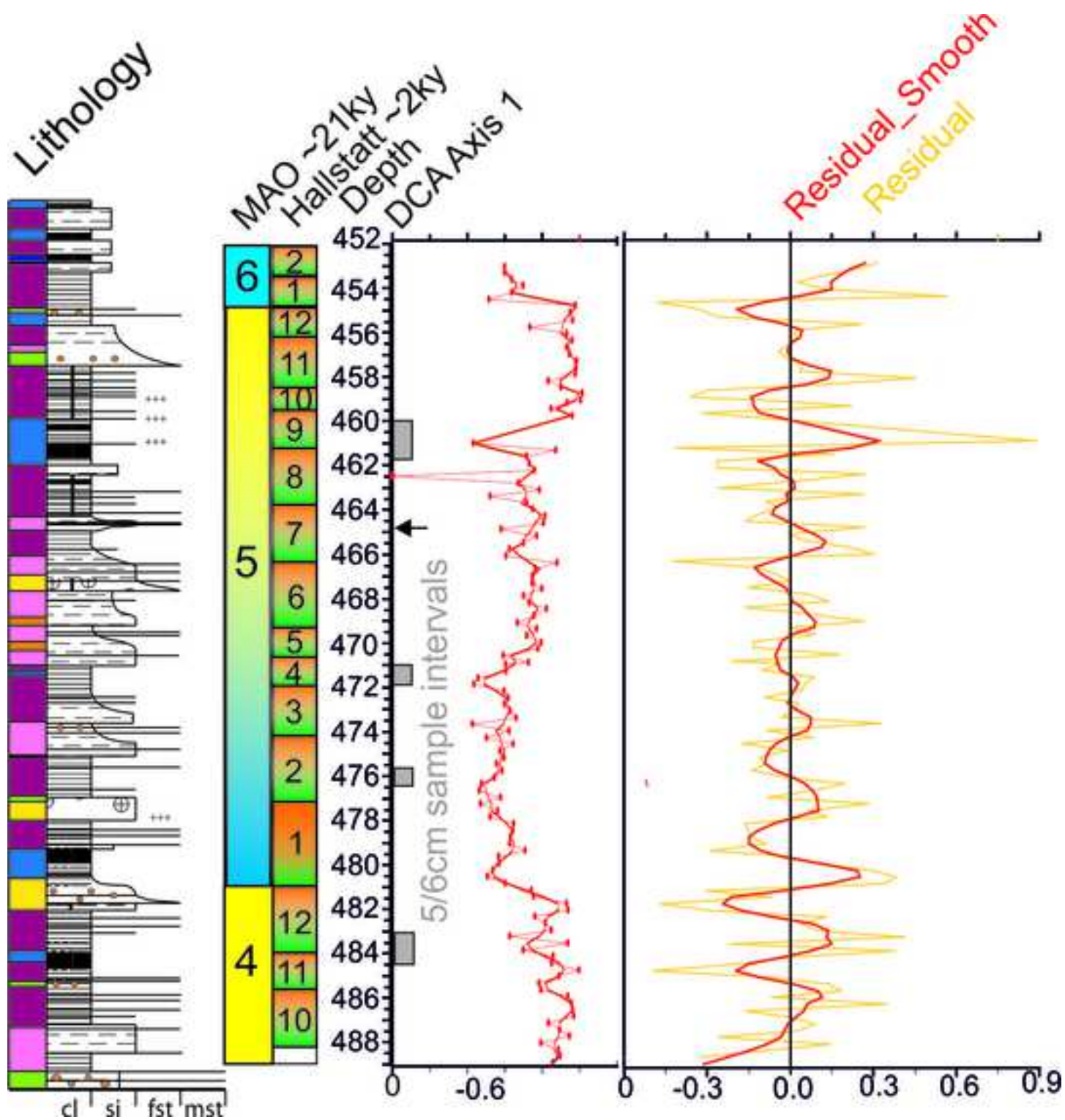
[Click here to download Figure Jolley et al Boltysch Fig 8.jpg](#) 





Figure





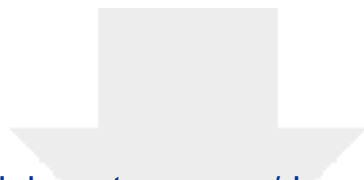


[Click here to access/download](#)

**Dataset**

[Jolley et al 30cm DCA Group sums Supp 3.csv](#)

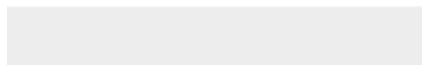
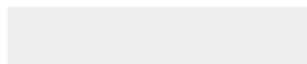




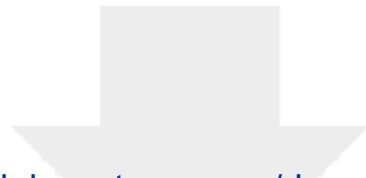
[Click here to access/download](#)

**Supplementary material (not datasets)**

Supporting data 1.jpg



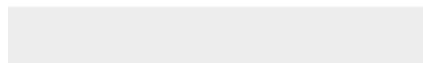
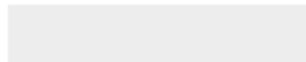


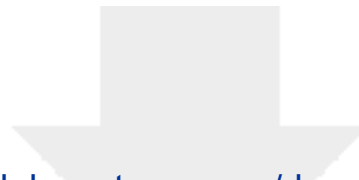


[Click here to access/download](#)

**Supplementary material (not datasets)**

Supporting data 2.jpg





[Click here to access/download](#)

**Supplementary material (not datasets)**  
Supplimentary data 3- core photos.jpg

